Multi-Model Identification of Pumping System in ASTANK2 Plant

Janetta CULIȚĂ, Dan ȘTEFĂNOIU

Automatic Control and Computer Science Department , "Politehnica" University of Bucharest
313 Splaiul Independentei, 060042, Bucharest, Romania
`janetta.culita@acse.pub.ro`
`dan.stefanoiu@acse.pub.ro`

Abstract—**This paper introduces a multi-model approach for the identification of the pumping (water distribution) system in a two-tank process, namely ASTANK2. An improved hill climbing algorithm is applied, in order to find the optimal structural indices of the identification models. A simulator that integrates the proposed numerical models and the analytical models developed in authors' previous work is implemented in MATLAB-SIMULINK environment. Its goal is to simulate the plant dynamics, according to various input scenarios, on one hand, and to validate the proposed model, on the other hand. Some simulation results are presented in the end.**

Keywords—double water tank system, identification model, hill climbing optimization, simulation.

I. INTRODUCTION

As an integrated part of the modern process industry, multitank systems incorporating water transportation circuits continues to capture the interest of the control engineering community, due to their nonlinear dynamics and multivariable character. This type of application offers a solid basis for illustrating many concepts in multivariable control [6]: designing multivariable optimal control techniques (derived from Distributed Model Predictive Control) [2], investigating robust observers used in Fault Detection and Isolation (FDI) ([8], [11]). In this respect, the modeling phase plays an essential role, providing an elementary support and a starting point for simulation studies, fault diagnosis and further control technique design.

The system decomposition method followed by expressing the analytical model of each component tank is generally approached in the literature, in order to construct the global mathematical model for the multitank installation. In some articles, linear numerical models are considered to represent the dynamic behavior of such a nonlinear system. For example, in [12], the model of a water tank process with smooth nonlinearity is built by combining Gaussian radial basis function networks with linear ARX models, in order to design and test various Model Predictive Control strategies. Although the quadruple tank process in [6] was successfully identified by an ARX model, the analytical model was preferred for investigating both the process properties and multivariable control. Moreover, the ARX model can be appropriate when the flow process exhibits small turbulences. Nevertheless, the analytical model is mostly encountered in the literature, regardless the shape of the tanks (rectangular, conical, spherical, cylindrical) their number (two, three, four [4] or five tanks [11]) and configuration.

This article mainly deals with the numerical modeling of the pumping system in a coupled tank plant, namely ASTANK2 [1], which was described in [3] and [5]. Practically, one continues here the work of [3], by reconsidering the analytical model of the water supply system feeding the main tanks, since it does not reflect the real evolution of the inlet flows of these tanks and consequently of the whole installation. Unlike the most plants described in the literature, where the water distribution system is controlled by three-way electro-valves, whose analytical model is well-known [2], in ASTANK2 one cannot accurately estimate the charge of the tanks, by applying the physics laws, as will be explained later. Therefore, operating with numerical models is undoubtedly a realistic requirement.

The paper is organized as follows. The next section shortly presents the ASTANK2 installation and introduce the motivation of approaching the numerical model. Section 3 describes the construction of the identification model for the upper horizontal pipes and presents an improved hill climbing algorithm, which is designed for searching the optimal structure of the parametric model. In the 4-th section, the plant simulation model is provided as a MATLAB/SIMULINK object, integrating both numerical model of the pipes and the analytical model of the tanks. Some simulation results compared to the real behavior are shown and discussed. Finally, section 5 concludes the paper.

II. IMPROVING ASTANK2 PLANT MODELING

A. Short presentation of the plant

The laboratory plant ASTANK2 is a two-tank coupled system, which is filled/drained by a flexible water delivery pipelines network, as illustrated in Figure 1. It has been designed for education and research purpose in modeling and control, by using safe industrial instrumentation. The upper tanks have different geometric shapes: tank 1 has a regular form (parallelepiped), whereas tank 2 has a sloped wall. The latter was designed in order to add nonlinearities in the dynamics of the plant. Both tanks are supplied/discharged from/into a storage reservoir (tank 3) located at the plant bottom, by means of a pumping and distribution network. Thus, the main pump is inverter-driven and delivers a variable water flow through the main vertical pipe, through supply frequency (and voltage) control.
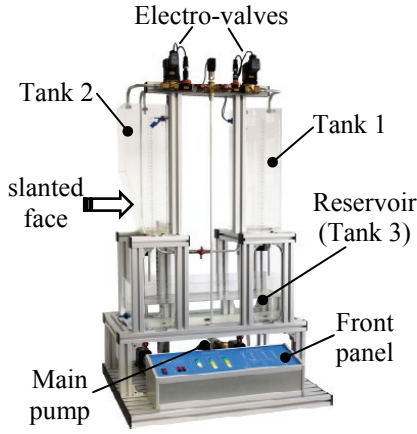
Fig. 1 ASTANK2 – a double-tank water installation

This pipe is branched at the upper side in two horizontal tubes, in order to fill up the main tanks. The inlet flow of each tank can be controlled by the corresponding *electro-valve* (EV), whose voltage is adjustable. The tanks can communicate to each other through a baseline pipe, which is acted by a manual tap (Figure 1). The plant also is endowed with flow and level transducers, level sensors, two auxiliary pumps and some manual taps, which allow the user to set various coupling configurations for the filling/drainage process and exhibits a wide range of experiments. The auxiliary pumps are ON/OFF and provide the main tanks with constant water flows when the taps on the secondary vertical pipes are open or partially open. A comprehensive description of ASTANK2 can be found in [3] and [5].

B. Multi-model approach

As presented in [3], the laboratory plant can be modeled by means of a multivariable system with five input commands (see Figure 2 below): the voltage on the main pump U, the voltages on the EV u_1 (for the right side tank 1) and u_2 (for the left side tank 2), the auxiliary pumps settings u_{01} (for the right side vertical pipe) and u_{02} (for the left side vertical pipe).
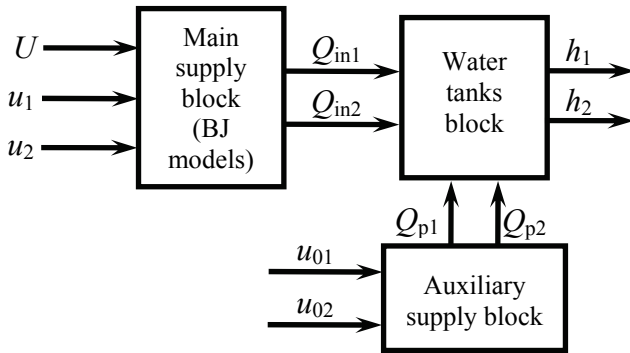

Fig. 2 Enhanced ASTANK2 functional blocks and signals

Two measurable outputs/states exist: h_1 (the water level in tank 1) and h_2 (the water level in tank 2). The input signals U, u_1 and u_2 vary within the range (0–10 V), while u_{01} and u_{02} are of type 0/1 (ON/OFF commands to be sent to the pumps). A simulation model based on the analytical equations of the component blocks (e.g. main and auxiliary pumps, short pipes, flow transducers, pressure transducer, flow control electro-valves and tanks) was developed and implemented in [3]. However, excepting for the tank block and auxiliary supply block, this model can be inadequate for expressing the real behavior of the global plant, since it does not take into account the physical (exploitation) constraints on the actual inlet flow of the tanks. Extended experimental investigations emphasized several practical limitations, as explained next.

a) The flow process in the upper horizontal pipes is very turbulent, because of their short length. In this case, the hydraulic phenomena are quite difficult to model and the discharge constants cannot be accurately estimated. Moreover, the differential pressure on the pipe cannot be measured, to construct the analytical model of the pipes.

b) Although the inlet flows of the tanks coming from the main pump can be adjusted by the input signals u_1 and u_2, the water volume pumped to the tanks is not necessarily distributed proportionally to the EV opening (voltages), especially when the difference between u_1 and u_2 is important (more than 4 V). For example, if $u_1 \geq 7$ V and $u_2 \leq 3$ V, the upper inlet flow of the tank 2 is negligible (practically, no water flows in the corresponding pipe). In this case, only the behavior of right side upper pipe can be modeled. This is a marginal situation that can be exploited separately. Consequently, in order to build accurate models of the upper short pipes one takes into account all the combinations of u_1 and u_2.

As a supplementary remark, in case of a marginal combination of u_1 and u_2, if the manual tap is open, the water accumulates in tank 2 only through the communication pipe from the tank 1, which can produce turbulences in the tank 2, especially when the current level of the water is bellow 2-3 cm.

c) Although the constructive parameters of the upper short pipes are approximately the same (the sections of the pipes are equal), the variations of the water flows in these pipes are not identical for symmetrical combination of u_1 and u_2. More specifically, the combination $u_1 = 7$ V and $u_2 = 8$ V does not provides the same models for the pipes as $u_1 = 8$ V and $u_2 = 7$ V. Therefore, all the voltage combinations have to be tested.

d) The voltage of the main pump, U, belongs to the interval $(0 \div 10)$ V. However, the minimum value necessary to fill the tanks by considering both EV completely open is $U_{\min} = 3.5$ V. The pump has an upper limit voltage as well, $U_{\max}$, below 10 V in some cases. As the experiments have shown, the real limits of U depends on the combination between u_1 and u_2. For example, for $u_1 = 6$ V and $u_2 = 4$ V, one measures $U_{\min} = 6.3$ V and $U_{\max} = 9$ V. Here, the upper limit was chosen in order to

avoid resonance (which enforced the pump to work in vibration mode). One has to mention here that such boundary values of the main pump voltage were experimentally fixed for each combination of the EV voltages u_1 and u_2.

e) When adjusting the voltage of an EV from the current value, the amplitude of change cannot exceed 3 V, otherwise, the EV can be damaged.

The issues above led to the enhanced functional block scheme of the installation, as depicted in Figure 2. The *main supply block* includes the vertical and horizontal short pipes, which distribute the water from the main pump directly to the upper tanks.

For the sake of simplicity, we can concisely refer it to as "the short pipes" block. It receives the control signals U, u_1, u_2 and provides the output signals Q_{in1} and Q_{in2} (the effective inlet flows of the tank 1 and tank 2, respectively). The *tank block* comprises all the three tanks of the plant and the *auxiliary supply block* is composed of the secondary constant flow pumps. As shown in the figure, the global output signals h_1 and h_2 are depending on the input signals Q_{in1}, Q_{in2}, Q_{p1} and Q_{p2}. The last two signals stand for the supplementary inlet flows yielded by the auxiliary pumps and are enabled by the input control signals u_{01} and u_{02}. A detailed description of these two blocks is presented in [3].

Following the practical restrictions, the short pipes block can be identified by using a multi-model approach which relies on the *Box-Jenkins* (BJ) models:

$$\begin{cases} y[n] = \dfrac{\mathrm{B}(q^{-1})}{\mathrm{F}(q^{-1})}u[n] + \dfrac{\mathrm{C}(q^{-1})}{\mathrm{D}(q^{-1})}e[n], \quad \forall n,m \in \mathbb{N}, \\ E\{e[n]e[m]\} = \lambda^2 \delta_0[n-m] \end{cases} \quad (1)$$

where the input signal stands for the pump voltage U, the output signal is Q_{in1} or Q_{in2}, the signal e represents a Gaussian white noise with unknown variance λ^2 and B, C, D, F are polynomials of degrees $nb+nk$, nc, nd, nf, respectively, with the intrinsic delay nk (usually, unit):

$$\begin{cases} \mathrm{B}(q^{-1}) = q^{1-nk}\left(b_1 q^{-1} + \cdots + b_{nb}q^{-nb}\right) \\ \mathrm{C}(q^{-1}) = 1 + c_1 q^{-1} + \cdots + c_{nc}q^{-nc} \\ \mathrm{D}(q^{-1}) = 1 + d_1 q^{-1} + \cdots + d_{nd}q^{-nd} \\ \mathrm{F}(q^{-1}) = 1 + f_1 q^{-1} + \cdots + f_{nf}q^{-nf} \end{cases}. \quad (2)$$

Thus, for each couple $\{u_1, u_2\}$, a BJ model can be estimated by generating the input signal U inside the associated interval $[U_{\min}, U_{\max}]$. This results in a map of distinct BJ models for each pipe, whose role is twofold: a) certainly, to simulate the dynamics of the plant for a prescribed input scenario

(specification of the input signals), by selecting the corresponding BJ model of the pipe from the available ones; b) to compute appropriate BJ models of the pipes for transitional combinations of $\{u_1, u_2\}$, by linearly interpolating the formerly built adjacent models, as explained in the sequel.

Figure 3 illustrates a part of a BJ model map, where the corners enclose already estimated models and can be interpreted as elements of a 2x2 matrix.
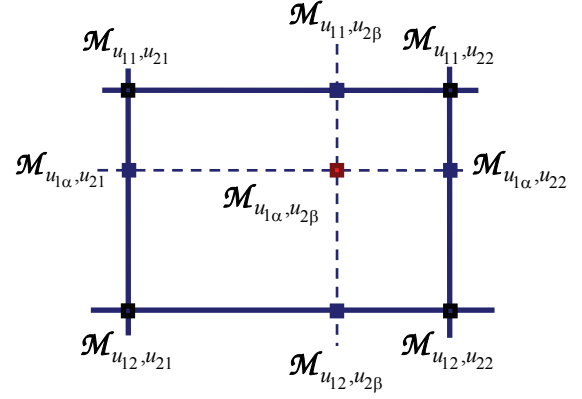

Fig.3 Model interpolation principle for specified EV settings

Obviously, such a model is located by the voltages u_1 and u_2 that set the EV openings. As the figure shows, a lattice of voltages can be set for each pipe. The generic cell of lattice is defined by two voltages for the left side EV (say u_{11} and u_{12}) and two voltages for the right side EV (say u_{21} and u_{22}). Four identification models associated to the current pipe have to be identified, by stimulating the plant with appropriate inputs. Such a model is denoted by $\mathcal{M}_{u_{1i},u_{2j}}$, where $i,j \in \{1,2\}$. Inside the cell, identification is not necessary, as models linear interpolation can be employed. Interpolating models means interpolating the coefficients of polynomials (2), according to offsets $\alpha, \beta \in [0,1]$ that define positions inside the cell. The offsets are uniquely defined by a couple of values $u_{1\alpha} \in [u_{11}, u_{12}]$ and $u_{2\beta} \in [u_{21}, u_{22}]$.

More specifically, the generic interpolation procedure consists of the following steps:

a) The offsets are computed by taking into account the coordinates of the corner and inner models:

$$\alpha = \frac{u_{12} - u_{1\alpha}}{u_{12} - u_{11}}; \quad \beta = \frac{u_{22} - u_{2\beta}}{u_{22} - u_{21}}. \quad (3)$$

b) Models corresponding to left and right sides of cell are obtained:

$$\begin{cases} \mathcal{M}_{u_{1\alpha},u_{21}} = \alpha \mathcal{M}_{u_{11},u_{21}} + (1-\alpha)\mathcal{M}_{u_{12},u_{21}} \\ \mathcal{M}_{u_{1\alpha},u_{22}} = \alpha \mathcal{M}_{u_{11},u_{22}} + (1-\alpha)\mathcal{M}_{u_{12},u_{22}} \end{cases}. \quad (4)$$

c) The final model results, eventually:

$$\mathcal{M}_{u_{1\alpha},u_{2\beta}} = \beta \mathcal{M}_{u_{1\alpha},u_{21}} + (1-\beta)\mathcal{M}_{u_{1\alpha},u_{22}}. \quad (5)$$

The interpolation operation can be applied when simulating the evolution of the flow process for intermediary input values $u_{1\alpha}$ and $u_{2\beta}$.

In multi-modeling approach based on lattices, it is suitable to reach the trade-off between the number of identification models and the validity of interpolation models. Obviously, if the lattice has too little nodes, then, although the identification effort is small, the distance between identification models could be too big and there is a high risk to work with invalid interpolated models. Conversely, if the lattice is too dense, then the interpolation models seemingly are valid, but the identification effort is significant. In case of ASTANK 2 pipes, a good compromise is obtained for $|u_{11} - u_{12}| = |u_{21} - u_{22}| = 1$ V.

C. Optimal identification of lattice

Identification of BJ models requires solving two optimization problems. If the polynomial degrees (the model structural indices) are known, then the coefficients can be estimated by means of Minimum Prediction Error Method [9], based on the quadratic criterion. To find the optimal structural indices of BJ models (i.e. the integers nb, nc, nd and nf) a granular optimization problem has to be solved. The optimization criterion defined below is referred to as *(model) fitness* and has to be maximized:

$$\mathcal{F}_N[nb, nc, nd, nf] = \frac{100}{1 + \dfrac{\sigma_\varepsilon}{\sigma_y}} \quad [\%]. \tag{6}$$

In definition (6), σ_y and σ_ε are standard deviations of the measured output (y) and prediction error (ε), respectively. Both signals are of length $N \in \mathbb{N}^*$. (Actually, $\sigma_y/\sigma_\varepsilon$ stands for the square root of SNR (*signal-to-noise ratio*).)

Since the criterion (6) generally exhibits fractal variations, with many local extremes, the problem of fitness maximization cannot be solved by exact optimization techniques. Therefore, a metaheuristic was employed in this aim. The optimization procedure belongs to *Hill Climbing Algorithms* (HCAs) [7], [10]. An improved version of basic algorithm was implemented, as described in the next section.

III. IMPROVED HILL CLIMBING ALGORITHM

It is well known that the local HCAs are designed to solve the following problem: a tourist tries to reach the top of a mountain starting from a certain altitude, without being informed on the path to follow. Obviously, the tourist is trying to solve the altitude maximization problem and needs to know how to estimate his/her vertical position at any time. The altitude is given by a cost function (e.g. the fitness (6)). The solution is based on a simple strategy: the tourist randomly searches a higher position to gain, compared to the previous one; each time he/she succeeds, he/she tries to keep that position and to avoid descending. The tourist stops climbing when at least one condition is met: a) the number of escaping from current position attempts is too big; b) the difference between two successive heights the tourist gained remains too small, after a number of successive attempts to improve the current position.

Denote by $\mathcal{F}$ the cost function (altitude) to be maximized, by $\mathcal{V}$ a bounded vicinity of the peak inside the finite searching space $\mathcal{S} \subset \mathbb{R}^{nx}$ (of size nx) and by $\mathbf{x}_0 \in \mathcal{V}$ the initial point to start the search. At each step, one evaluates the tourist's next position $\mathbf{x}_{k+1} \in \mathcal{V}$ from the current one $\mathbf{x}_k \in \mathcal{V}$, by selecting a direction at random. (In order to avoid being captured by a local maximum, from time to time, the tourist can jump to another vicinity, different from $\mathcal{V}$.) More specifically, the next position is evaluated as follows:

$$\mathbf{x}_{k+1} = \mathbf{x}_k + \Delta\mathbf{x}_{k+1}, \quad \forall k \in \mathbb{N}, \tag{7}$$

where $\Delta\mathbf{x}_{k+1}$ is an offset that have to be set such that $f(\mathbf{x}_{k+1}) > f(\mathbf{x}_k)$. One way to do this is to generate the offset through some *uniformly distributed pseudo-random sequences generator* (U-PRSG), which is specific to Monte-Carlo method. Since this approach leads to a time consuming numerical procedure (as the tourist is blindly searching for a direction to move), another strategy was innovated. The tourist could be allowed to have a compass, in order to roughly select his/her direction of attack. This compass is available through the local gradient of search surface, as this vector (or its opposite) can point to a peak.

More specifically, from the current position $\mathbf{x}_k$ ($k \in \mathbb{N}$), after generating the offset $\Delta\mathbf{x}_{k+1}$ through the U-PRSG, one estimates the gradient of the possible path to follow:

$$\nabla\mathcal{F}_{k+1} = \left[\frac{\mathcal{F}(\mathbf{x}_{k+1}) - \mathcal{F}(\mathbf{x}_k)}{x_{k+1,1} - x_{k,1}} \quad \cdots \quad \frac{\mathcal{F}(\mathbf{x}_{k+1}) - \mathcal{F}(\mathbf{x}_k)}{x_{k+1,nx} - x_{k,nx}} \right]^T. \tag{8}$$

By default, any null denominator in definition (8) will set to null the corresponding gradient component. In this way, the gradient set the orientation of the next direction to follow, which speeds up the searching. Practically, now:

$$\mathbf{x}_{k+1} = \mathbf{x}_k + \nabla\mathcal{F}_{k+1}, \quad \forall k \in \mathbb{N}. \tag{9}$$

Actually, the recursive equation (9) was inspired by basic gradient (Cauchy) method from exact optimization techniques. As already known, the Cauchy method has modest accuracy, but provides a simple numerical procedure. Therefore, another improvement made to the basic HCA is to introduce an adaptive advancement step α, in order to control the searching speed on the direction pointed by the gradient (8). Thus, the next position to take can be the following:

$$\mathbf{x}_{k+1} = \mathbf{x}_k + \alpha_{k+1}\nabla\mathcal{F}_{k+1}, \quad \forall k \in \mathbb{N}, \tag{10}$$

where α_{k+1} is evaluated such that the next possible position remains in the vicinity $\mathcal{V}$ and the optimal position is approached faster than by simply using the gradient (with unit advancement step – see equation (9) again).

The improved HCA is summarized next.

1. Input data

➢ Search vicinity $\mathcal{V}$ (equations allowing the user to decide whether a point belongs or not to this set).

➢ Altitude indicator, $\mathcal{F}$ (criterion to maximize).

➢ Maximum number of attempts to escape from current position, N.

➢ Maximum number of attempts to find a better position than the current one, M.

➢ Threshold to detect staying on the same height, $\varepsilon > 0$.

2. Initialization

a. Use a U-PRSG to select the tourist departure position $\mathbf{x}_0 \in \mathcal{V}$.

b. Evaluate the altitude of departure point: $\mathcal{F}(\mathbf{x}_0)$.

c. Set the initial gradient for the departure point, $\nabla \mathcal{F}_0 \in \mathbb{R}^{nx}$ (usually, $\nabla \mathcal{F}_0 = \mathbf{0}$).

d. Set the initial advancement step, $\alpha_0 \in \mathbb{R}$ (usually, $\alpha_0 = 1$).

e. Set a counter for the number of attempts to escape from the current position: $n = 0$.

f. Set a counter for remaining at the same height: $m = 0$.

g. Set the starting iterations index: $k = 0$.

3. Approaching the peak. For $k \geq 0$:

3.1. Attempting to escape from the current position:

    3.1.1. Use the U-PRSG to generate an offset: $\Delta \mathbf{x}_k^{k+1}$.

    3.1.2. While $\mathbf{x}_k + \Delta \mathbf{x}_k^{k+1} \notin \mathcal{V}$, calibrate the U-PRSG to generate a new offset inside the hyper-cube $\left[\mathbf{0}, \Delta \mathbf{x}_k^{k+1}\right]$, where $\Delta \mathbf{x}_k^{k+1}$ is the most recently generated offset.

    3.1.3. Set the proposed position $\mathbf{x}_k^{k+1} = \mathbf{x}_k + \Delta \mathbf{x}_k^{k+1} \in \mathcal{V}$ and evaluate its altitude: $\mathcal{F}\left(\mathbf{x}_k^{k+1}\right)$.

    3.1.4. Estimate the gradient corresponding to the proposed position by using $\mathbf{x}_k$ and $\mathbf{x}_k^{k+1}$ in definition (8). Thus, one obtains $\nabla \mathcal{F}_{k+1}$, which is stored in memory.

    3.1.5. Estimate the optimal advancement step by the recurrence: $\alpha_{k+1} = \alpha_k - \left(\nabla \mathcal{F}_{k+1}\right)^T \nabla \mathcal{F}_k$ (see [10]). Obviously, the previous gradient, $\nabla \mathcal{F}_k$, can be found in memory.

    3.1.6. While $\mathbf{x}_k + \alpha_{k+1} \nabla \mathcal{F}_{k+1} \notin \mathcal{V}$, calibrate the U-PRSG to generate a new advancement step in $\left[0, \alpha_{k+1}\right]$, where α_{k+1} is the most recently generated step (starting from the optimal advancement step of 3.1.5.).

    3.1.7. Set the final offset: $\Delta \mathbf{x}_{k+1} = \alpha_{k+1} \nabla \mathcal{F}_{k+1}$.

3.2. Test whether the altitude could increase or not if the tourist would move to the new position:

    3.2.1. Evaluate the altitude of the proposed position: $\mathcal{F}\left(\mathbf{x}_k + \Delta \mathbf{x}_{k+1}\right)$.

    3.2.2. If $\mathcal{F}\left(\mathbf{x}_k + \Delta \mathbf{x}_{k+1}\right) > \mathcal{F}\left(\mathbf{x}_k\right)$, then:

        3.2.2.1. Allow the tourist to move into the new position: $\mathbf{x}_{n+1} = \mathbf{x}_n + \Delta \mathbf{x}_{n+1}$. (Note that the altitude has already been evaluated: $\mathcal{F}\left(\mathbf{x}_{k+1}\right) = \mathcal{F}\left(\mathbf{x}_k + \Delta \mathbf{x}_{k+1}\right)$.)

        3.2.2.2. Reset the counter related to blocking on the same position: $n \leftarrow 0$.

        3.2.2.3. If $\left\|\nabla \mathcal{F}_k\right\| < \varepsilon$, then the tourist practically keeps the same altitude and the corresponding counter increases: $m \leftarrow m + 1$.

        3.2.2.4. Otherwise, reset the corresponding counter: $m \leftarrow 0$.

    3.2.3. Otherwise, the tourist has to conserve the current position ($\mathbf{x}_{k+1} = \mathbf{x}_k$) and the blocking counter increases: $n \leftarrow n + 1$.

3.3. If $n > N$ or $m > M$, stop the search and go to the final stage.

3.4. Otherwise, proceed with the next iteration: $k \leftarrow k + 1$.

4. Output data

➢ The tourist current position: $\mathbf{x}_{k+1}$.

➢ The tourist current altitude, $\mathcal{F}\left(\mathbf{x}_{k+1}\right)$, assumed to approximate the hill peak height.

Although the overall performance of improved HCA is inferior to other metaheuristics, it can offer an acceptable trade-off between speed and accuracy. Moreover, the numerical procedure is easy to implement on a regular computer, without special needs. The procedure can be run 2-3 times, with different departure positions, in order to increase the chance to find the highest peak.

The most adequate BJ model can be found following the HCA strategy. One defines the tourist position by the vector of structural indices $\mathbf{x} = \begin{bmatrix} nb & nc & nd & nf \end{bmatrix}^T$. Obviously, the cost function $\mathcal{F}$ to maximize is the fitness $\mathcal{F}_N$, as defined in equation (6). It is however necessary to outline that, in this case, the tourist position is defined by non negative integer coordinates. Thus, each time a new position is proposed, the rounding to the nearest integer has to be applied. (This operation does not appear in the procedure above.)

IV. IMPLEMENTATION OF MODEL AND SIMULATION RESULTS

In order to build the model map for each pipe, the BJ models were built for each combination of EV openings, as controlled by the couple of voltages $\{u_1, u_2\}$. As already mentioned, the lattice nodes are set for integer values of voltages, selected in the interval [3-10] V. Note that when $u_1 \leq 3\,\mathrm{V}$ and $u_2 \leq 3\,\mathrm{V}$ the pipe models cannot accurately be identified, because the limitations described in section II. For

other combinations, when $u_1 \leq 3$ V and $u_2 > 3$ V only the models for the right side pipe can be estimated, while for $u_1 > 3$ V and $u_2 \leq 3$ V only the models for the left side pipe can be estimated.

The input signal U was generated as a *normally distributed pseudo-random sequence* (PRS) with values in the specified interval $[U_{\min}, U_{\max}]$. Moreover, the change between two successive step values of U was limited to [0.5,5] V. The duration of a randomly generated value varies from 14 s to 24 s, in order to avoid misusing the pump, on one hand, and to produce turbulences that affect the measured values provided by the flow transducer, on the other hand. The output data were acquired during 20 minutes with a sample period $T_s = 0.5$ s. Clearly, the plant has to be stimulated with different input signals for each voltages combination $\{u_1, u_2\}$, both on identification and validation purposes.

The maximum values of BJ model structural indices were set to $Nb = Nc = Nd = Nf = 30$. The input parameters of the HCA were set as follows: the maximum number of attempts to escape from current position – $N = 200$; the maximum number of attempts to find a better position than the current one – $M = 20$; the threshold to detect the staying on the same height – $\varepsilon = 10^{-2}$. Usually, the algorithm completes in about two hours for each model on a regular PC.

In order to construct and simulate the model of the right side pipe for a transient combination $\{u_{1\alpha}, u_{2\beta}\}$, one has first to identify the four neighboring combinations of $\{u_{1\alpha}, u_{2\beta}\}$ and then to interpolate the already identified models attached to the each lattice node. For example, following the notations in Figure 3 and equations (3)-(5), for $u_{1\alpha} = 8.5$ V and $u_{1\beta} = 8.3$ V, one obtains $u_{11} = 8$ V, $u_{12} = 9$ V, $u_{21} = 8$ V, $u_{22} = 9$ V, $\alpha = 0.5$ and $\beta = 0.7$. Table I shows the optimal structural indices and the corresponding fitness values $\mathcal{F}_N^{\max}$ obtained with the HCA, for each lattice node like in Figure 3, corresponding to right side pipe.

TABLE I

Node models structure of the right side pipe for $u_{1\alpha} = 8.5$ V and $u_{2\beta} = 8.3$ V

$\{u_1, u_2\}$ [V]	$\mathbf{x}_{\max}^T$	$\mathcal{F}_N^{\max}$ [%]
{8,8}	$[5 \quad 10 \quad 21 \quad 16]$	86.94
{8,9}	$[3 \quad 14 \quad 21 \quad 30]$	86.56
{9,8}	$[5 \quad 12 \quad 30 \quad 7]$	85.56
{9,9}	$[5 \quad 11 \quad 30 \quad 11]$	85.91

On the right side of Figure 4, variations of simulated versus measured input flows Q_{in1}, for each optimal model in Table I, are depicted. The interpolated model is then obtained by using equations (4)-(5). In order to test and validate this model, one has to compare the data obtained by simulating the interpolated model with the data acquired for the specified intermediary point. Thus, the plant is first stimulated with a PRS U, (different from all PRS generated to perform node models identification), as illustrated in the right side of Figure 5. The validation outcome is displayed on the right side of Figure 6. Note that the inflow variation obtained by simulating the interpolated model is quite close to the measured inflow, as expressed by the corresponding fitness: $\mathcal{F}_N^{\{8.5, 8.3\}} = 85.06$ %. As expected, this value is slightly smaller than the fitness values of the four adjacent models. (Recall that the input PRS has changed!) This confirms the validation of the interpolated model of the right side pipe for $u_{1\alpha} = 8.5$ V and $u_{1\beta} = 8.3$ V.

Similarly, one can identify and validate an intermediary model for the left side pipe. Thus, for $u_{1\alpha} = 8.3$ V and $u_{1\beta} = 8.6$ V, one obtains $u_{11} = 8$ V, $u_{12} = 9$ V, $u_{21} = 8$ V, $u_{22} = 9$ V, $\alpha = 0.7$ and $\beta = 0.4$. The features of the optimal adjacent models are given in Table II.

TABLE II

Node models structure of the left side pipe for $u_{1\alpha} = 8.3$ V and $u_{2\beta} = 8.6$ V

$\{u_1, u_2\}$ [V]	$\mathbf{x}_{\max}^T$	$\mathcal{F}_N^{\max}$ [%]
{8,8}	$[9 \quad 12 \quad 19 \quad 20]$	85.13
{8,9}	$[12 \quad 19 \quad 17 \quad 26]$	86.38
{9,8}	$[11 \quad 14 \quad 29 \quad 24]$	86.57
{9,9}	$[13 \quad 4 \quad 14 \quad 7]$	87.22

On the left side of Figure 4, one can see the variations of simulated versus measured input flows Q_{in2}, for each optimal model in Table II. Following the same identification steps as in case of the right side pipe, one obtains the interpolated model of left side pipe, for the aforementioned intermediary voltages combination. In order to validate this model, the plant is stimulated with a PRS U, as shown in the left side of Figure 5. Finally, the validation of interpolated model is proven by the variations depicted in the left side of Figure 6. This time too, one can see that the input flow obtained by simulating the interpolated model is close to the measured inflow. The corresponding fitness is: $\mathcal{F}_N^{\{8.3, 8.6\}} = 85.27$. This validates the the interpolated model of the left side pipe for $u_{1\alpha} = 8.3$ V and $u_{1\beta} = 8.6$ V.

The identified numerical models are integrated with the analytical model of the water tanks in SIMULINK environment, as stated in section II (see Figure 2 again). This led to the global simulator illustrated in Figure 7. After simulating the plant behavior with the integrated interpolation models, water level data were acquired and compared to the simulation results. In Figure 8, left side and right side level variations are depicted. As one can notice, the simulator stays close to the ASTANK2 plant. The fitness values of simulated levels are of 78.51% (for the right side tank) and of 80.44% (for the left side tank). This is quite a satisfactory performance that successfully completes the ASTANK2 modeling phase.
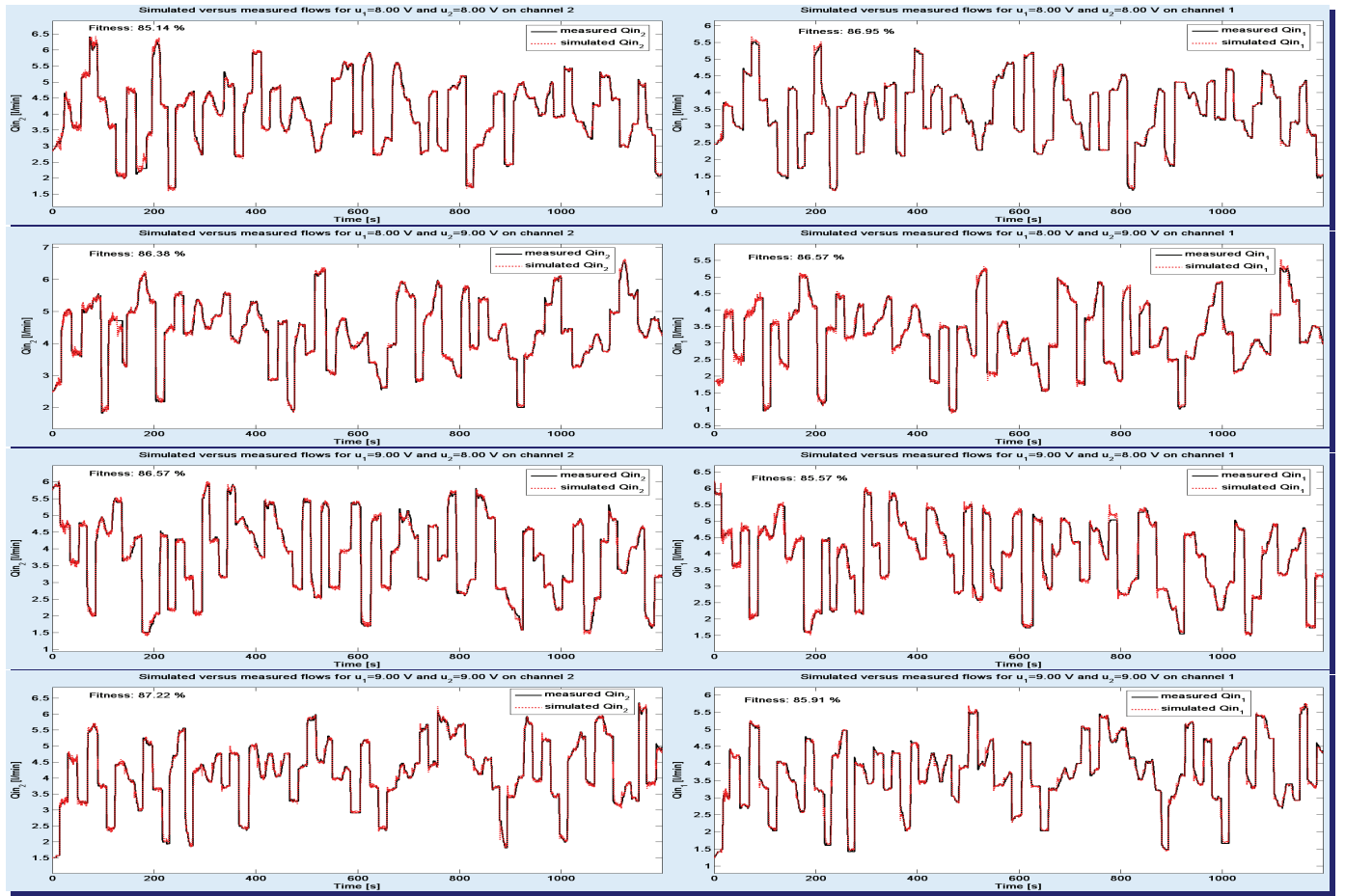
Fig.4 Lattice node models performance for the left side and right side pipes (same order as in Tables I and II)
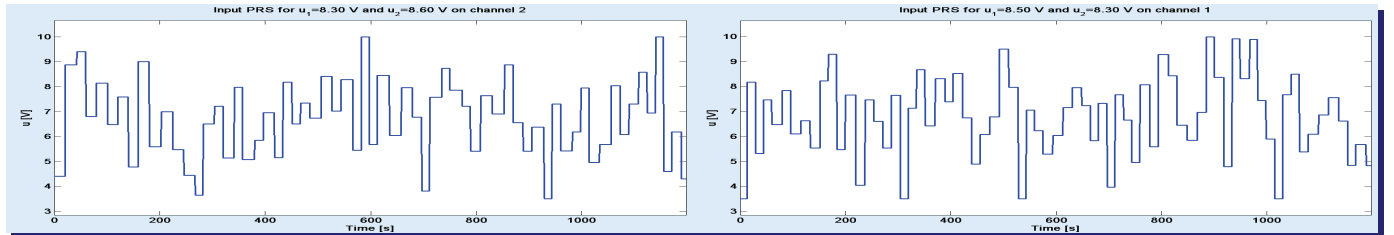

Fig.5 Inputs (PRS) stimulating the left side and right side pipes, in order to perform inner models validation
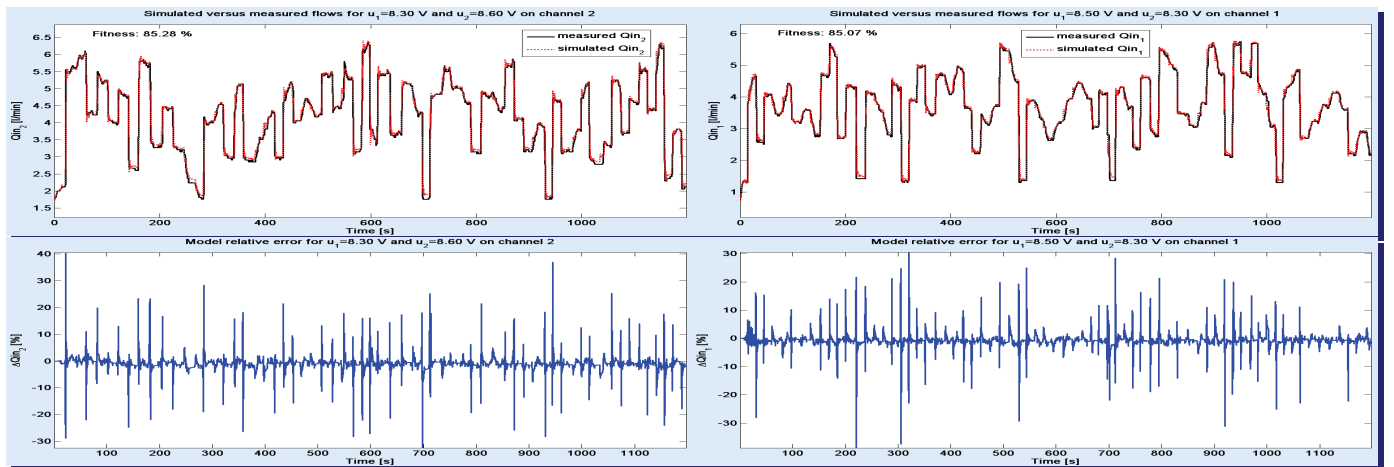

Fig.6 Inner models performance for the left side and right side pipes (inflows up, errors bottom)
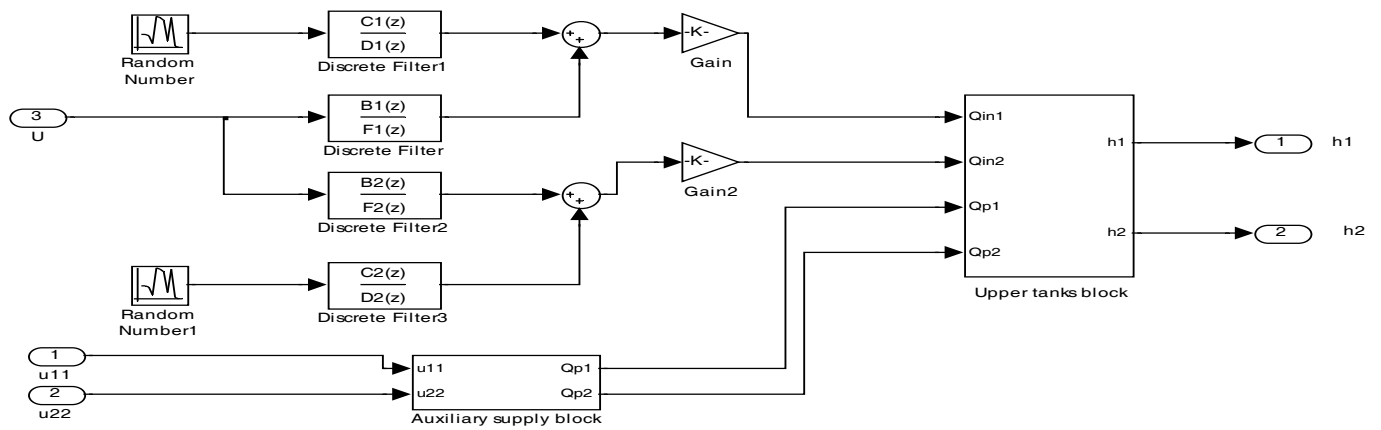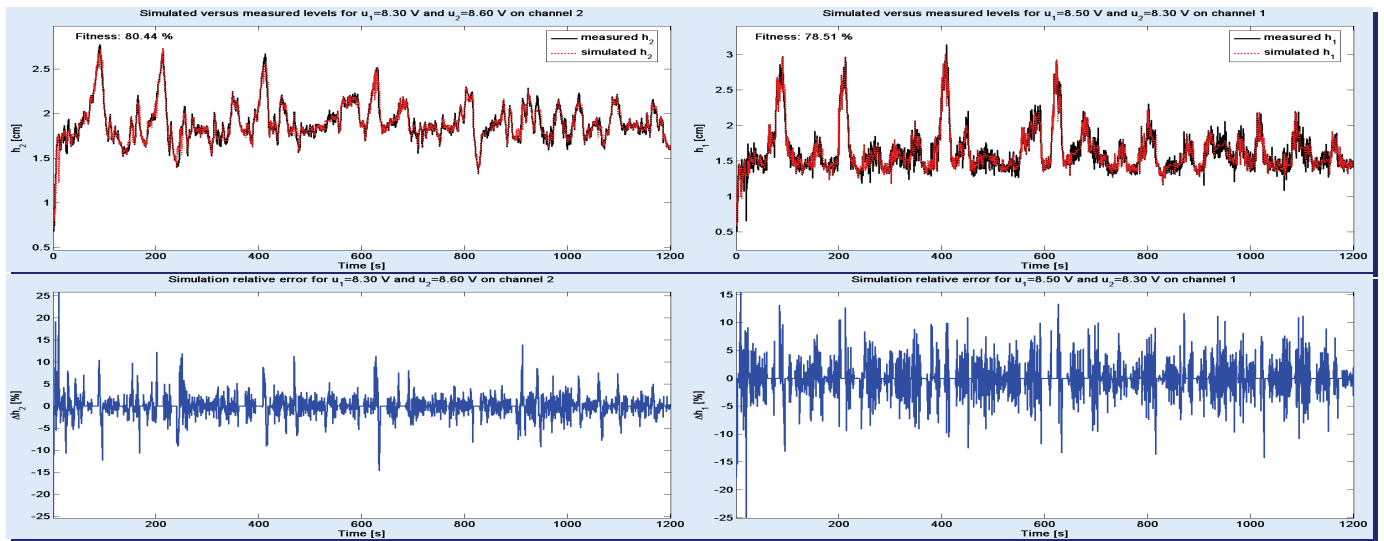
Fig.7 Simulink block diagram of ASTANK2 installation

Fig.8 ASTANK2 simulator performance: measured versus simulated water level on left side and right side tanks (up) and corresponding errors (bottom).

V. CONCLUSIONS

The paper describes an improved simulation model of ASTANK2 plant, which combines numerical and analytical mathematical models. The identified numerical models were tested and validated for different input configurations. Moreover one proves that we can compute models for any combination of EV input voltages by interpolating the available ones. The combined modeling approach seems to be promising for simulating the real behavior of the plant, based on which various control techniques can be verified.

REFERENCES

[1] ASTI Automation, "Technical handbook of double water tank system".

[2] Alvaradoa I., Limona D., Muñoz de la Peña D. et al., "A Comparative Analysis of Distributed MPC Techniques Applied to the HD-MPC Four-Tank Benchmark", in *Journal of Process Control*, Vol. 21, Issue 5, pp. 800–815, June 2011.

[3] Culita J., Stefanoiu D., Dumitrascu A., "ASTANK2: Analytical Modeling and Simulation", in *Proceedings of the 20-th International Conference on Control Systems and Computer Science*, Bucharest, Romania, pp. 141-148 (Vol. 1)., May 27–29, 2015.

[4] Dormido S., Esquembre F. "A quadruple-tank process: an interactive tool for control education", *Proceedings of the European Control Conference (ECC),* April, 2003.

[5] Dumitrascu A., Istratescu C., Stefanoiu D., Culita J. "Environment Communication and Control Systems Integrated on Teaching Platforms – Case Study: Double Water Tank System", ", in *Proceedings of the 20-th International Conference on Control Systems and Computer Science*, Bucharest, Romania, pp. 941-945 (Vol. 2), May 2015.

[6] Johansson K.H., "The Quadruple-Tank Process: A Multivariable Laboratory Process with an Adjustable Zero", *IEEE Transaction on Control System Technology*, vol. 8, no. 3, May 2000.

[7] Russel S.J., Norvig P. *Artificial Intelligence – A Modern Approach*, Prentice Hall, Upper Saddle River, New Jersey, U.S.A, 1995.

[8] Salim M., Khosrowjerdi M.J. "Data-driven H∞ Controller/Detector Design for a Quadruple Tank Process", *Journal of Control Engineering and Applied Informatics*, Vol.19, No.1 pp. 3-14, 2017.

[9] Soderstrom T., Stoica P. *System Identification*, Prentice Hall, London, U.K., 1989.

[10] Stefanoiu D., Borne P., Popescu D., Filip Gh.F., El Kamel A. *Optimization in Engineering Sciences – Metaheuristics, Stochastic Methods and Decision Support*, John Wiley & Sons & ISTE Press, London, U.K., 2014.

[11] Tahraou S., Meghebbar A., Boubekeur D., Boumédiène A. "System Modeling and Faults Diagnosis of a Five Hydraulic Tank", *Journal of Control Engineering and Applied Informatics*, Vol.18, No.1 pp. 59-67, 2016.

[12] Zhou F., Peng H., Qin Y.M., Zeng X.Y., Xie W.B., Wu J. "RBF-ARX model-based MPC strategies with application to a water tank system", *Journal of Process Control*, Vol. 34, pp. 97-116, October 2015.